Sigma Journal of Engineering and Natural Sciences
Web page info: https://sigma.yildiz.edu.tr
DOI: 10.14744/sigma.2026.2146

Research Article

A conformal 4-element phased array antenna using a T-junction power divider for beam steering in X-band unmanned aerial vehicle applications

Okan EVREN[1], Sena Esen BAYER KESKİN[2,*], Nurhan TÜRKER TOKAN[3]

[1]*Turkish Aerospace, Ankara, 06980, Türkiye*
[2]*Department of Electrical and Electronics Engineering, Kırklareli University, Kırklareli, 39000, Türkiye*
[3]*Department of Electronic and Communications Engineering, Yildiz Technical University, İstanbul, 34220, Türkiye*

ARTICLE INFO

Article history
Received: 22 April 2025
Revised: 18 June 2025
Accepted: 11 July 2025

Keywords:
Beam Steering; Phased Array Antenna; T-Junction Power Divider; UAVs; X-Band

ABSTRACT

This paper presents a 4-element conformal phased array antenna with beam steering capabilities designed for mounting on unmanned aerial vehicles (UAVs) for X-band applications. The antenna integrates a T-junction power divider to achieve electronically steered beams and reduce side lobe levels. The design features a 1×4 array with optimized parameters, "S"-shaped structures for beam steering, and tapered lines for impedance matching that transition logarithmically from 100Ω to 50Ω to ensure effective signal transmission. The proposed array antenna has a size of 70 mm × 50 mm and a thickness of 1.57 mm. Consequently, the array antenna achieves a reflection coefficient of -30.91 dB with a bandwidth of approximately 250 MHz, centered at 10.3 GHz, and a gain of 10.28 dBi, oriented at $\theta = 0°$. In addition, for surface compatibility analysis, the phased array antenna is bent on a cylinder with a radius of 133 mm for analysis and measurements. The experimental results confirm the antenna's suitability for X-band UAV applications.

Cite this article as: Evren O, Bayer Keskin SE, Türker Tokan N. A conformal 4-element phased array antenna using a T-junction power divider for beam steering in X-band unmanned aerial vehicle applications. Sigma J Eng Nat Sci 2026;44(5):3107–3119.

INTRODUCTION

Throughout history, wars have been shaped by the background, experience and doctrines of the past. However, due to the multidimensional and complex nature of today's warfare technology, environments need to be analyzed and considered in every aspect. In environments such as land, sea, air and space, manned and unmanned weapons, vehicles and robots are currently used as the critical components in contemporary warfare. Thanks to today's technology, long-term plans for unmanned systems to be used in military operations are actively in progress [1, 2]. As a result of the developments in recent years, unmanned aerial vehicles have taken their place in the war environment. They are known to be actively used not only in defense technologies, but also in various fields such as agriculture [3, 4], logistics [5-7], telecommunications [8, 9], disaster management [10, 11] and smart city applications [12]. Based on the altitude,

*Corresponding author.
*E-mail address: senakeskin@klu.edu.tr

This paper was recommended for publication in revised form by Editor-in-Chief Ahmet Selim Dalkilic

Published by Yıldız Technical University Press, İstanbul, Turkey
© Author. This is an open access article under the CC BY-NC license (http://creativecommons.org/licenses/by-nc/4.0/).

UAVs are generally classified as hand-held, Close, NATO, Tactical, Medium Altitude Long Endurance (MALE), High Altitude Long Endurance (HALE) and Hypersonic [13]. Although UAVs are known to be able to operate unmanned in concept, they need to communicate with the ground control station on the ground. This communication allows command and control, payload data and weapon control to be provided instantaneously. The transmitted data enables the professional teams at the ground control station to make the right decision and timing to use the aircraft for its intended purpose [14-16]. UAVs are equipped with multiple antennas, serving various functions such as communication with the ground control station and supporting transmission of the data between payload systems and avionics equipments [17]. The positioning of each antenna on the aircraft is critical since radiation characteristics of the antennas are affected by the environmental conditions. As an example, antennas for communication with ground control station are positioned to the lower part of the aircraft, while GPS antennas are located to the upper parts [18].

The capabilities of UAVs are evaluated in direct proportion to the payloads they carry. In this context, Electro-Optical/Infra-Red (EO/IR) cameras, electronic warfare systems, radar systems and weapons are considered as payloads. Recently, usage of Synthetic Aperture Radars (SARs) became popular for topographic monitoring and mapping of the landscape in UAVs. It is able to operate regardless of daylight and weather conditions [19, 20]. Besides a wide range of applications in the military field, the SAR systems are also commonly used in geology [21], disaster prevention [22], airborne SAR systems [23], and meteorological observation [24]. Extending the operating time of the aircraft in the air is one of the primary considerations in avionics engineering. Therefore, studies have been carried out to improve factors such as aerodynamic structure, weight and power consumption of the aircraft in order to increase the hover time [25, 26].

Due to their low profile, compact size and easy fabrication, microstrip antennas [27-29] are actively used in a wide range of applications such as aviation [30-32], space [33], automotive [34, 35], sensor systems [36, 37]. The ability of microstrip antennas to meet the bandwidth and high gain demands and application of them in different shapes with different feeding methods have made them diverse in terms of usage [38]. They can also be used in the form of arrays to demonstrate different radiation characteristics. With the array antenna structure, it is possible to shape antenna parameters such as directivity, gain and side lobe level and steer the beam [39].

Within the scope of this paper, a synthetic aperture radar system (SAR) antenna is introduced for the UAVs. A microstrip antenna scanning system, which can be considered equivalent to the SAR system, has been designed in conformal form to detect and track potential targets and produce high-resolution radar images for target classification and land topography formation in all weather conditions. The planar and low-weight structure of the conformal array also supports to increase the duration of UAVs in the air and make them capable of performing longer missions during operation. The paper introduces a more efficient and lightweight alternative to currently used mechanically steered, bulky radar system that is designed to be used on air platforms for intelligence, reconnaissance-surveillance, suppression and attack operations. As an example of the NxN conformal array, a 1x4 element phased array antenna prototype utilizing a T-junction power divider is fabricated and concept of beam steering is demonstrated experimentally. The simulation and measurement results show that proposed design offers a practical solution for UAVs, reducing weight and aerodynamic drag, thereby increasing operational efficiency and extending hover time, while still providing effective radar performance for SAR applications in the X-band.

CONFORMAL PHASED ARRAY ANTENNA FOR UNMANNED AERIAL VEHICLES

Conformal Phased Array Antenna (PAA) is ideal for advanced communications, remote sensing, and radar imaging applications in UAV systems, particularly in scenarios requiring electronic beam steering capabilities. Figure 1 illustrates the electronic beamforming scenarios, highlighting interactions among UAVs equipped with conformal PAAs, base stations, fixed-wing and rotary-wing UAVs, satellites, and ground radar. Ground radar and base stations work with UAVs to monitor and manage airspace or conduct targeted data collection. The conformal PAA enables UAVs to perform electronic beamforming, allowing dynamic steering of radar beams and communication links without physical movement of the antenna. This capability

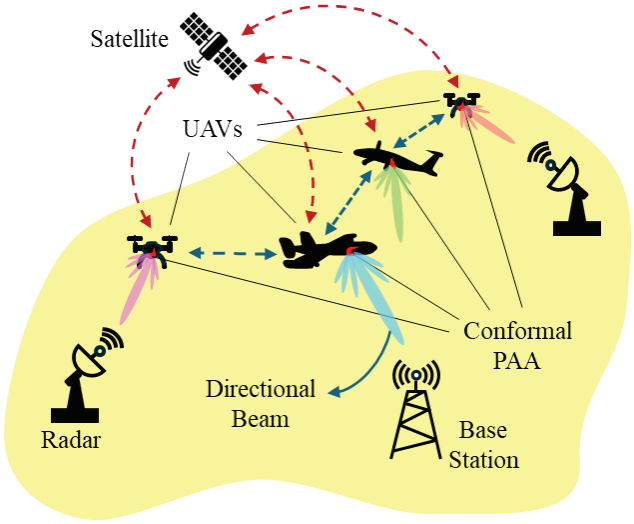


Figure 1. Illustration of electronic beamforming application scenarios for UAVs with PAA.

is crucial for covering large areas, tracking moving targets, focusing on specific targets, real-time surveillance, high-resolution imaging, and secure, seamless data transfer. The number of elements, N, in the PAA significantly influences its beamforming performance. As the number of elements increases, the antenna's ability to scan across wider angles and achieve finer beam resolution improves. For example, an NxN conformal array can be integrated onto the UAV surface, enabling advanced beam scanning capabilities. As a specific application example, this paper presents a 4x4 element conformal PAA that offers a practical solution for efficient beam steering in UAV applications, providing improved control over signal directionality and range.

Conformal NxN Array Antenna Design

An array antenna structure is designed to achieve specific directivity and polarization characteristics by positioning and configuring multiple radiating elements. In this study, a methodology for N×N array antenna is introduced, utilizing unit patch antennas fed by coaxial transmission lines. The unit element is a microstrip antenna with a gain of approximately 7 dBi within the frequency range of 8-12 GHz. The unit patch has dimensions of 9.53 mm in width and 7.33 mm in length, with a frequency bandwidth of 2.52 GHz between 9.88 and 12.4 GHz. The antennas within the array are positioned such that the distance between adjacent feed points is λ/2. This generalized NxN array antenna design approach can be applied to various configurations, allowing for adjustments in spacing and overall dimensions based on specific requirements. To reduce drag effect on the aircraft, a surface-compatible design is employed. The antenna is bent to conform to the cylindrical surface of the airframe, which is formed by a circular section with radius R and an elliptical section with axis lengths R1 and R2. Positioned at the bottom of the airframe, the antenna fits the circular section with radius R, as illustrated in Figure 2. By considering the physical dimensions of the well-known UAVs, R, R1 and R2 values are determined as 185 cm, 89 cm and 133 cm, respectively. These values are accounted for the bending criteria of the conformal phased antenna array.

Beam Steering with the Conformal Phased Antenna Array

Electronic beam steering enables directional control of the antenna without physical movement by manipulating the radiation pattern through adjustments in the phase and amplitude of the antenna feed. Effective beam steering necessitates the introduction of a phase difference between antenna elements. This phase difference can be achieved by incorporating a phase shifter into the antenna design, as illustrated in Figure 3. In this work, a power divider designed in accordance with T-junction power divider principles is employed to control the phase of the antenna array elements of a array fed by a microstrip transmission line-fed unit antenna is designed for X-band applications.

In electronic beam steering, increasing the number of antenna elements proportionally enhances the array's directivity and gain. However, in lossy environments, the gain peaks after a certain number of elements and subsequently

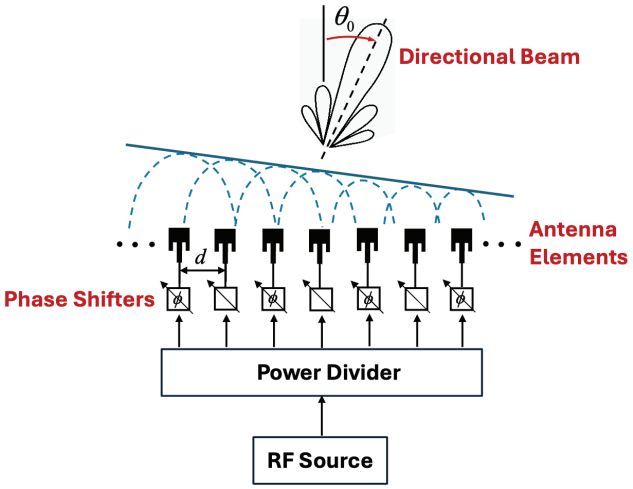


Figure 3. Phased array antenna mechanism.

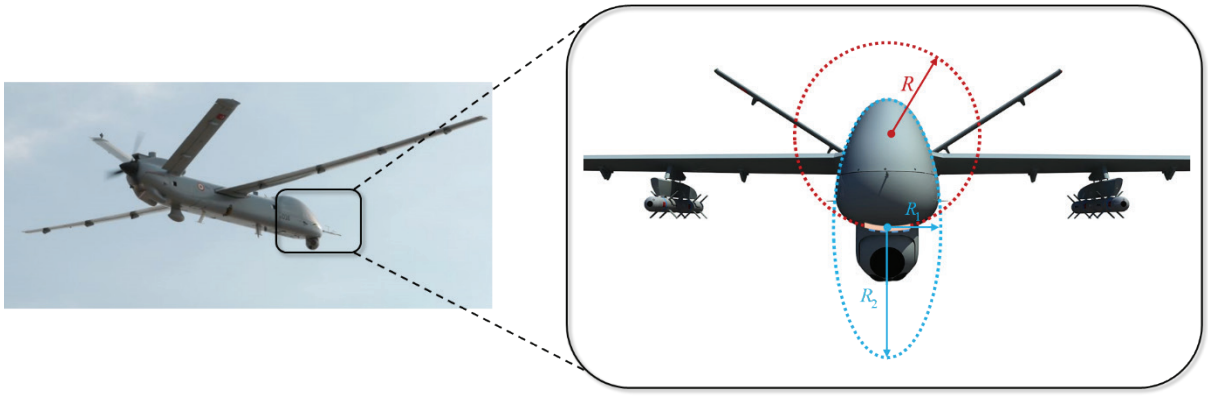


Figure 2. The demonstration and problem space definition of the conformal phased array on the UAV.

decreases. Phased array antennas can scan rapidly by feeding each element with appropriate phase values, eliminating mechanical constraints. Assuming identical elements with half-wavelength spacing and uniform feed, applying the same phase shift to all elements results in a main beam perpendicular to the antenna surface due to zero relative phase difference. Introducing a relative phase difference steers the main beam. For a beam shift by θ_0, the phase difference is $\Delta\emptyset = 2\pi(d/\lambda)sin\theta_o$. Thus, the phase values for each element are given by $\Delta\emptyset + m\,\Delta\emptyset$, where $m = 0,1,2,\ldots,(N - 1)$ [40].

Beam Steering with a Conformal 4x4 Array Antenna

As an example of the concept presented above, a 4 x 4 array antenna comprising microstrip antennas with coaxial feeds is generated. The top and bottom views of the PAA are shown in Figure 4a and b, respectively. The centers of the coaxial feeds are spaced 15 mm ($\lambda_0/2$ at 10 GHz) apart both horizontally and vertically, resulting in an overall antenna array dimension of 63.2 x 63.2 mm^2 ($W \times L$). To obtain the conformal array, the planar array is bent over the surface of a cylindrical structure with a radius of R.

Figure 5a presents the S11 parameters for both the PAA and the conformal PAA. The PAA, designed for the X-band with a center frequency of 10 GHz and a bandwidth of approximately 450 MHz (spanning from 9.8 GHz to 10.25 GHz), has a return loss level of 24.2 dB at the center frequency. The conformal PAA exhibits a similar bandwidth of approximately 400 MHz. Analysis of the PAA's far-field radiation pattern, as shown in Figure 5b, reveals that the main beam is directed at $\theta = 0°$ with a gain of 17.13 dBi. The side lobe level and the 3 dB beamwidth of the pattern are 13.9 dB and 24.9°, respectively at $\phi = 0°$ plane, whereas they are 13.7 dB and 25.2° at $\phi = 90°$ plane. Bending the antenna to fit the cylindrical surface of the airframe resulted in a gain reduction of 0.44 dB. However, the gain level of 16.69 dBi achieved with the conformal PAA remains sufficient for the targeted UAV. As illustrated in Figure 5c, similar to the PAA antenna, the side lobe level is around 11 dB, and the 3 dB beamwidth is approximately 25.5° at $\phi = 0°$ plane, whereas they are 13.4 dB and 25.2° at $\phi = 90°$ plane.

Figure 6a presents the beam scanning results for both the PAA and the conformal PAA, with the main beams directed at 5° intervals in the $\phi = 0°$ plane. Here, θ represents the radiation direction, while ϕ denotes the azimuth angle. The normal of the aircraft surface, where the phased array is located aligns with the z-axis. When the beam is steered to $\theta = 45°$, there is a 1.17 dB reduction in gain for the PAA and a 1.86 dB reduction for the conformal PAA compared to the gain at $\theta = 0°$, and 1.8 dB and 1.41 dB for the planar and conformal arrays, respectively in the $\phi = 90°$ plane. Generally, patterns with gain values exceeding 15 dB can effectively radiate to the desired angle. Figure 6b shows the results for beam scanning in the $\phi = 90°$ plane over an angular range of $-45° \leq \theta \leq 45°$, with the main beams steered at 5° intervals. The results are similar to those obtained in the $\phi = 0°$ plane. Analysis of the side lobe levels in Figure 6 reveals the following: In the $\phi = 0°$ plane, the side lobe level for the PAA at $\theta = 5°$, is 19.46 dB, decreasing to 14.22 dB at $\theta = 45°$. For the conformal PAA in the same plane, the side lobe levels are 12.41 dB at $\theta = 5°$, and 6.64 dB at $\theta = 45°$. In the $\phi = 90°$ plane, the side lobe level for the PAA is 17.9 dB at $\theta = 5°$, and 13.53 dB at $\theta = 45°$. For the conformal PAA, the side lobe levels are 13.03 dB at $\theta = 5°$, and 8.86 dB at $\theta = 45°$.

An Application Example: Conformal 1x4 Phased Array Design with T-Junction Power Divider

To demonstrate the beam steering performance of the conformal array experimentally, three 1x4 phased arrays consisting of patch unit elements are designed to radiate towards three different directions (towards $\theta = 0°$, 15° and -20° in $\phi = 0°$ plane). T-junction power divider is used for

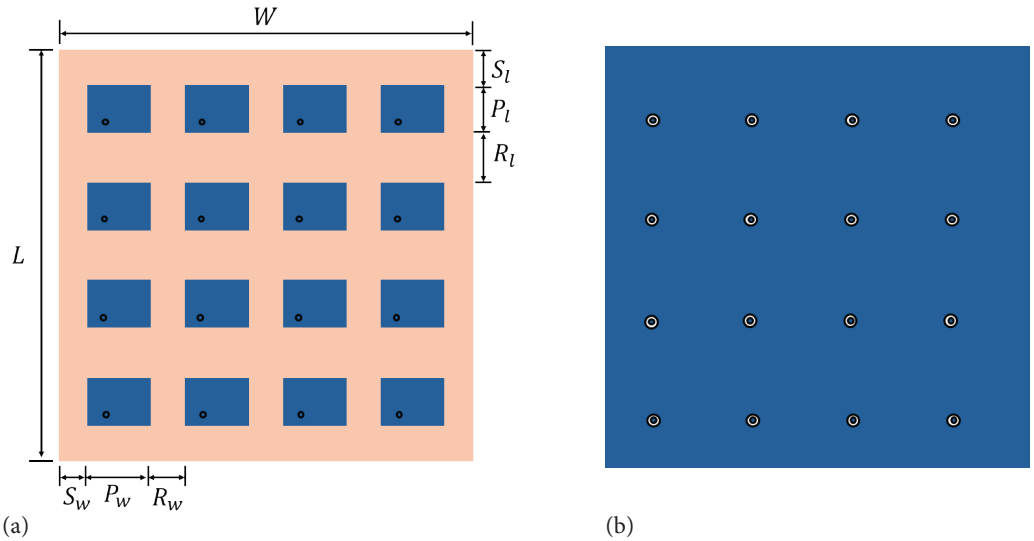
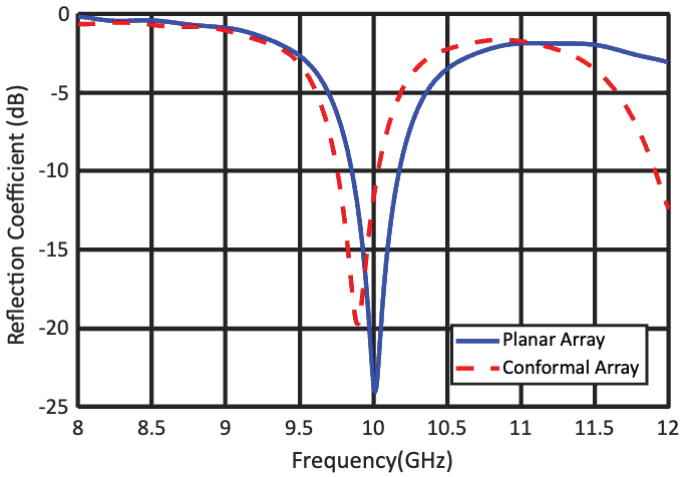
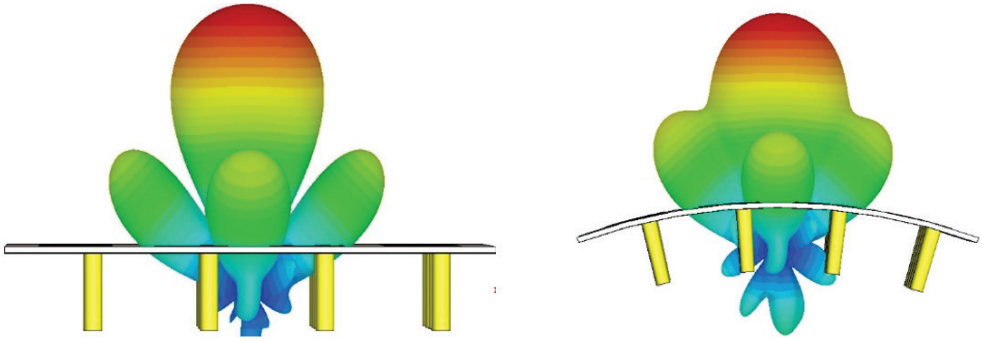


Figure 4. 4x4 microstrip array antenna (a) Top view of the PAA; (b) Bottom view of the PAA.



(a)



(b) (c)

Figure 5. Radiation characteristics of the 4x4 planar and conformal array (a) Reflection coefficient; (b) 3D gain of the planar PAA; (c) 3D gain of the conformal PAA.

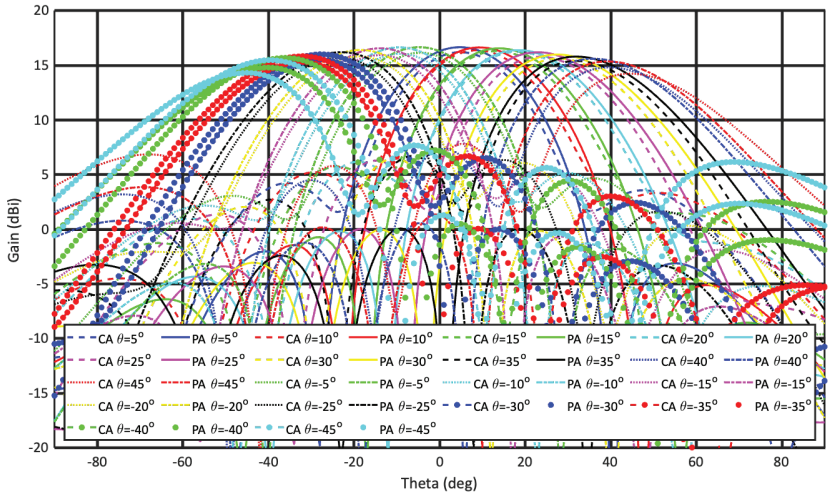
the feeding network of the arrays. Corresponding phases of the antennas are achieved by adjusting the lengths of the transmission lines.

T-junction power divider

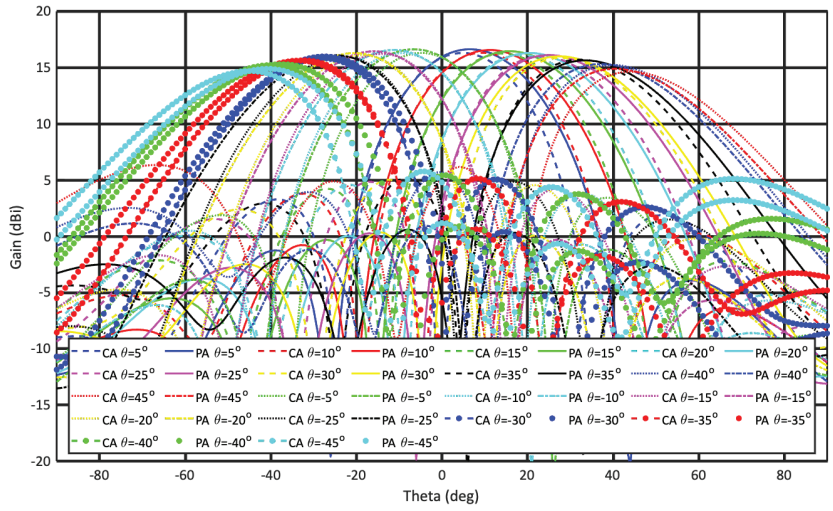
T-junction power dividers have been widely studied in the literature and have a wide range of applications, such as multiband dividers [41, 42], filter dividers [43, 44] and harmonic suppression dividers [45]. The advantages of T-junction power dividers, such as low cost and simple manufacturing, make them preferred in array applications. Another advantage is the isolation between input and output ports [46, 47]. T-junction power divider circuits are composed of quarter-wavelength transmission lines with varying characteristic impedance values [48]. A $\lambda/4$ transformer is used for impedance matching. For characteristic impedance matching, the quarter-wave transmission line must have an impedance of $\sqrt{2}Z_0$, so that all the ports are matched to impedance Z_0 [49]. The 1x4 phased array with a T-junction power divider is shown in Figure 7a. It is composed of a 1x4 microstrip array, located above the red dashed line for signal radiation, while a T-junction power divider, positioned below the dashed line, is employed to control the phase of the antenna array elements. The geometric dimensions of the 1x4 phased antenna array with a T-junction power divider are presented in Table 1. The output phase variation of the T-junction power divider in the 8 GHz to 12 GHz frequency band is shown in Figure 7b. It is

Table 1. Geometric dimensions of the 4-way inphase T-junction power divider

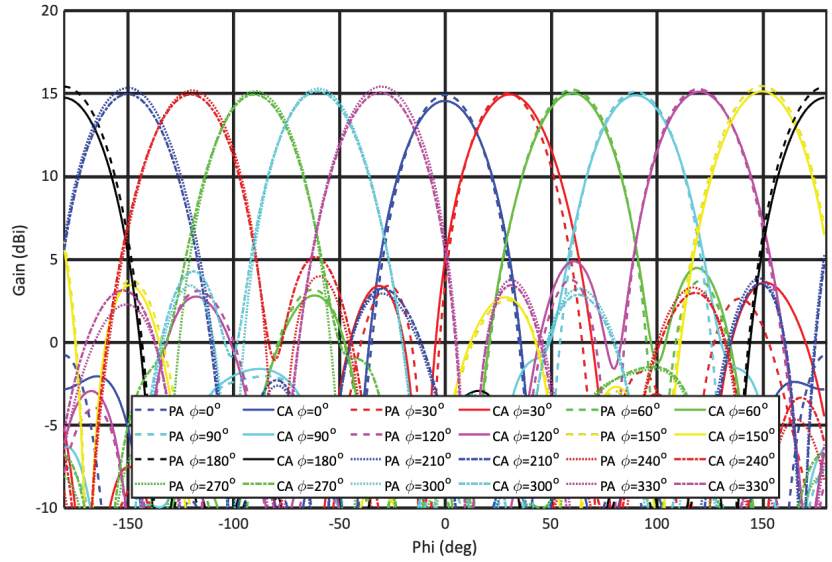
Parameter	S_{l1}	S_{l2}	S_{l3}	S_{l4}	S_{l5}	S_{w1}	S_{w2}	S_{w3}	S_{w4}
Value (*mm*)	1.3	2	2	2	2	2	2	2	2
Parameter	t_w	t_l	l_W	l_t	f_{l1}	fl_2	b_l	D_W	D_{fl}
Value (*mm*)	4.8	6.5	4.3	1.4	1.12	1.12	2	70	32.36



(a)

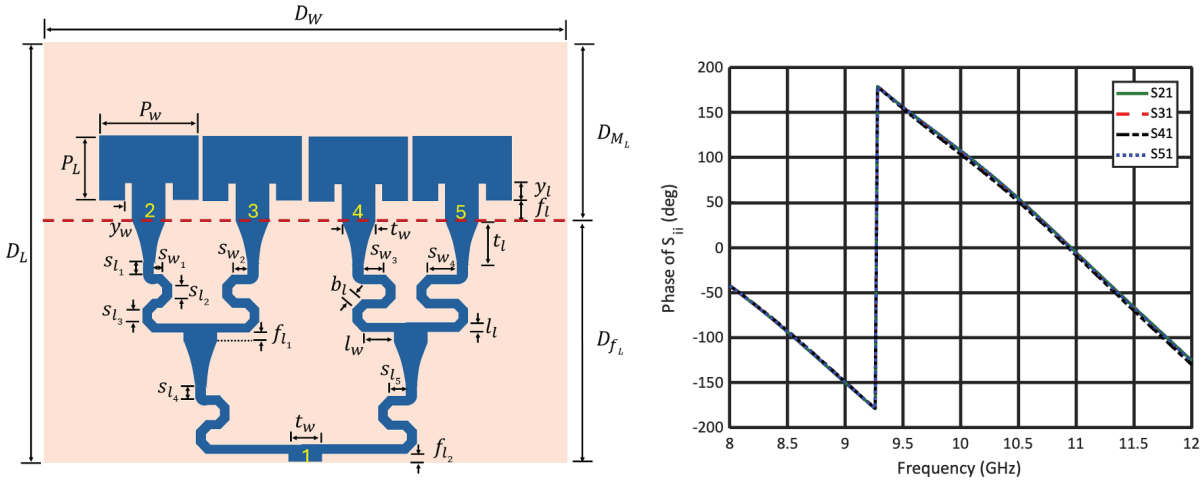


(b)



(c)

Figure 6. Beam steering performance of the planar and conformal array (a) $\phi = 0°$ plane; (b) $\phi = 90°$ plane; (c) $\theta = 45°$ plane.



(a) (b)

Figure 7. 1x4 phased array with the power divider (a) schematic view with design parameters; (b) output phases.

observed that the phases of the four output ports are almost equal within the band. The impedance of each output port is 50Ω. The "S" shaped structures, required for beam steering to different angles, have an impedance of 100Ω. The tapered transmission lines, which are used for the transition logarithmically from 100Ω to 50Ω, are used to ensure smooth impedance matching and minimize reflections, enhancing bandwidth and reducing insertion loss.

1x4 T-junction power divider, which incorporates tapered lines for connection to the microstrip antenna and S-shaped lines for interconnecting the tapered sections, significantly impact the phase shifts of the output signals. Variations in the dimensions of S_{l5}, S_{w1}, S_{w2}, S_{w3}, and S_{w4} alter the effective electrical length and impedance characteristics, thereby modifying the propagation delays and resulting phase relationships at the outputs.

Beam Steering with the 1x4 Phased Array

Beam orientation towards θ = 0°

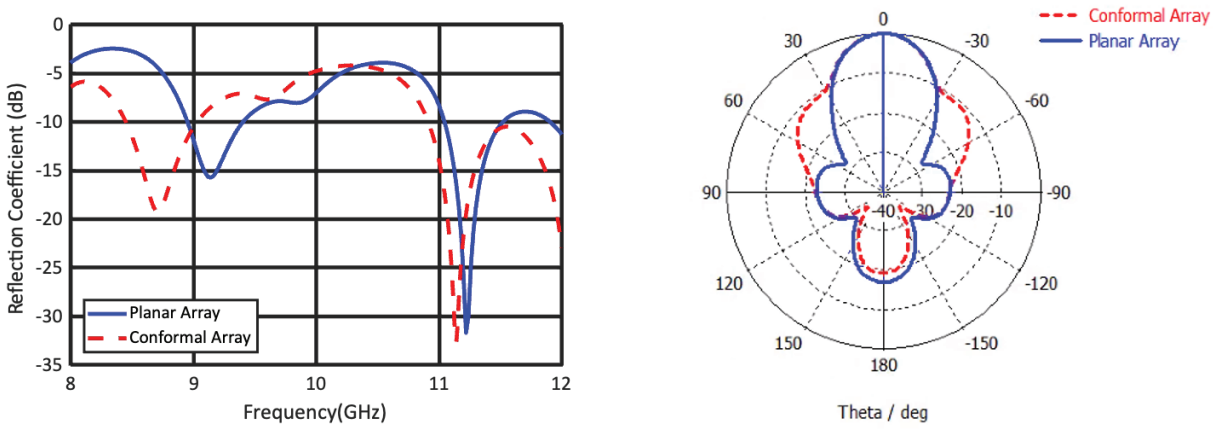
The dimensions of the 1x4 PAA directed at $\theta = 0°$ are presented in Table 2. Very similar results are obtained when compared to a 1x4 planar microstrip-fed array antenna without a T-junction power divider. Reflection coefficient variation of the planar and conformal 1x4 phased arrays are given in Figure 8a. The T-junction power divider, which is used to adjust the input phases of the array elements, results in a frequency shift for both arrays. Although the bandwidth remains almost the same for the planar array, the lower operation frequency of the array has been reallocated to the upper region of the X-band. The normalized gain patterns of the arrays are demonstrated in Figure 8b, for the arrays oriented towards $\theta = 0°$. It is observed that radiation patterns show very similar characteristic within the 10 dB beamwidth of the pattern. The one-dimensional directivity plot, the antenna array achieved a gain of 10.28 dBi, with the main beam directed at $\theta = 0°$. The side lobe level was around -10 dB, and the half-power beamwidth was measured to be 24.3°.

Beam orientation towards θ = 15°

The geometric dimensions of the 1x4 PAA oriented at 15°, with modifications to the dimensions S_{l5}, S_{w1}, S_{w2}, S_{w3}, and S_{w4}, are presented in Table 3. The antennas aligned along the x-axis require a phase shift of approximately 46° to achieve beam steering at an angle of $\theta = 15°$, following the formula $\beta_x = -kd_x sin\theta cos\phi$ which defines the phase shift necessary for beam steering in an array antenna. Here, B_x represents the phase shift required for the antenna elements aligned along the x-axis to achieve the desired beam steering, k denotes the wavenumber, d_x indicates the spacing between the antenna elements along the x-axis, θ and ϕ are the angles representing the elevation angle at which the beam is steered, and the azimuth angle of the steering direction, respectively. Based on this calculation, the phase at port S_{21}, the second output port, is measured as 321°. The phase at port S_{31}, the third output port, differs by 46° from the second port, resulting in a phase of 275°.

Table 2. Geometric dimensions of the 1x4 PAA, oriented towards $\theta = 0°$

Parameter	f_l	y_l	y_w	P_L	P_W	D_W	D_L	D_{Ml}
Value (mm)	2.5	2.4	1	9.4	14.12	70	50	17.63



(a) (b)

Figure 8. Performance of the planar and conformal 1x4 phased arrays designed to radiate towards θ = 0° (a) reflection coefficient; (b) normalized gain patterns.

Table 3. Geometric dimensions of the 1x4 PAA, oriented towards θ = 15°

Parameter	S_{l1}	S_{l2}	S_{l3}	S_{l4}	S_{l5}	S_{w1}	S_{w2}	S_{w3}	S_{w4}	t_w	t_l	l_W	l_t
Value (*mm*)	1.3	2	2	2	2.5	1.25	2.3	3.15	4.35	4.8	6.5	4.3	1.4
Parameter	f_l	f_{l1}	fl_2	b_l	y_l	y_w	P_L	P_W	D_W	D_L	D_{Ml}	D_{fl}	
Value (*mm*)	2.5	1.12	1.12	2	2.4	1	9.4	14.12	70	50	17.63	32.26	

Similarly, the phase values at the remaining ports, S_{41} and S_{51}, were analyzed to be 229° and 183°, respectively, maintaining the same phase difference. Output phases of the 4-way T-junction simulated in CST for radiating towards θ = 15° are illustrated in Figure 9. Figure 10 shows the simulated reflection coefficient and normalized gain patterns of the planar and conformal 1 x 4 phased arrays designed to radiate towards θ = 15°. Although radiation towards θ = 15° is expected, the main beam direction of the patterns shows 1° of disorientation.

Beam orientation towards θ = -20°

The geometric dimensions of the 1x4 PAA oriented at -20°, with modifications to the dimensions S_{l5} , S_{w1} , S_{w2}, S_{w3}, and S_{w4}, are presented in Table 4. The antennas require a phase shift of approximately -61° to achieve beam steering at an angle of θ = -20°, as defined by the phase shift formula. The phase value at port S_{21}, is measured at 155°, while the phase at the S_{31} is found to be 216°. The phase values at the remaining two ports are calculated at 277° and 338°, respectively. Output phases of the 4-way T-junction simulated in CST for radiating towards θ = -20° are illustrated in Figure 11. Figure 12 shows the simulated reflection coefficient and normalized gain patterns of the planar and conformal 1 x 4 phased arrays designed to radiate towards θ = -20°. Although the input phases of the array are adjusted to steer the mean beam towards θ = -20°, the full wave analysis result shows that the main beam is oriented towards θ = -18°. This slight disorientation is attributed to minor phase differences between the inputs of the array as demonstrated in Figure 11.

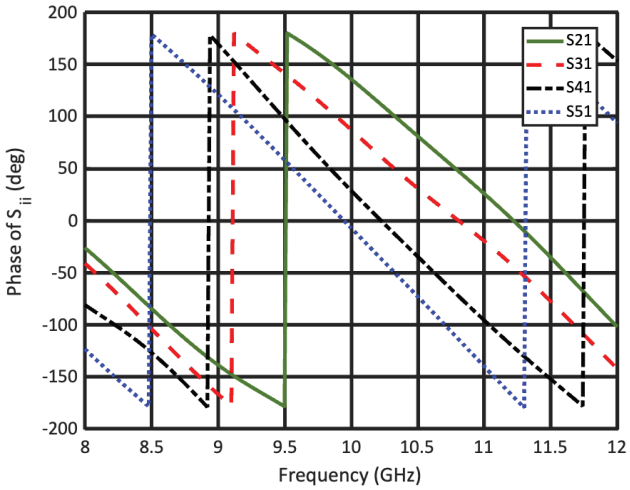
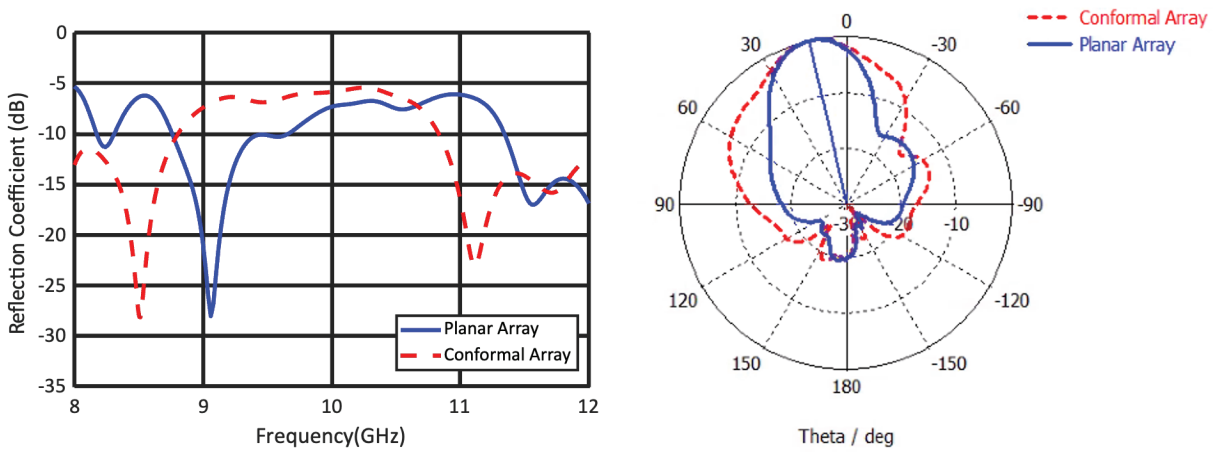


Figure 9. Output phases of the 4-way T-junction for radiating towards θ = 15°.



(a) (b)

Figure 10. Performance of the planar and conformal 1x4 phased arrays designed to radiate towards $\theta = 15°$ (a) reflection coefficient; (b) normalized gain patterns.

Table 4. Geometric dimensions of the 1x4 PAA, oriented at $\theta = -20°$

Parameter	S_{l1}	S_{l2}	S_{l3}	S_{l4}	S_{l5}	S_{w1}	S_{w2}	S_{w3}	S_{w4}	t_w	t_l	l_W	l_t
Value (*mm*)	1.3	2	2	2	1.5	4.2	2.7	3.5	2.2	4.8	6.5	4.3	1.4
Parameter	f_l	f_{l1}	fl_2	b_l	y_l	y_w	P_L	P_W	D_W	D_L	D_{Ml}	D_{fl}	
Value (*mm*)	2.5	1.12	1.12	2	2.4	1	9.4	14.12	70	50	17.63	32.26	

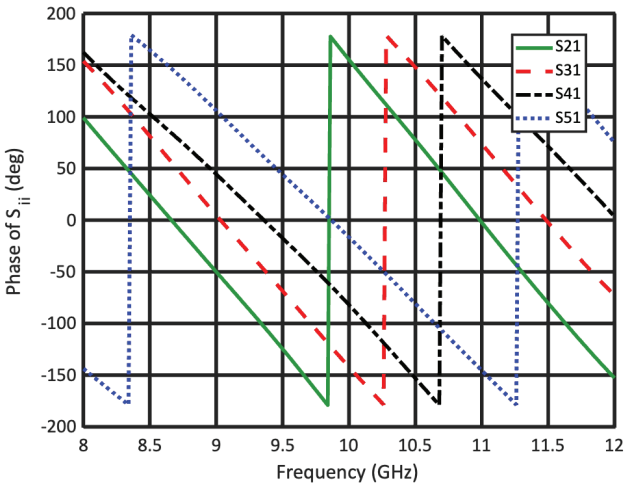


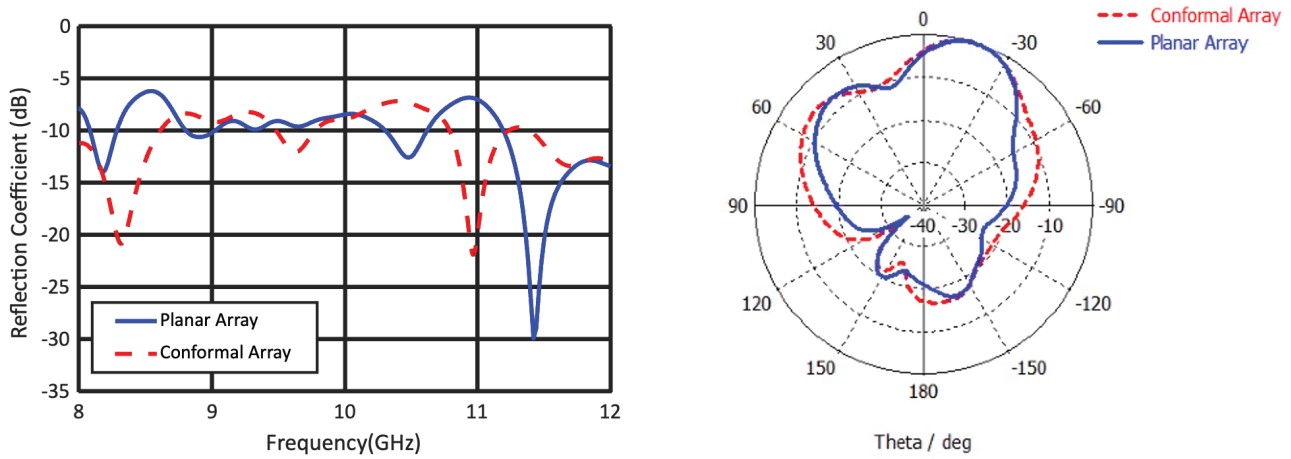
Figure 11. Output phases of the 4-way T-junction for radiating towards $\theta = -20°$.

Experimental Verification

To demonstrate the beam steering performance of the conformal arrays, the 1x4 arrays whose input phases are arranged to radiate towards $\theta = 0°$, 15° and -20° are fabricated by chemical etching technique. The prototype of the conformal arrays with the T-junction power divider circuits are given in Figure 13. The conformal structure of the arrays is generated by bending the planar array on a cylindrical surface whose radius is equal to R parameter as given in Figure 2. The arrays and the feeding network were fabricated on Rogers RT5880 substrate ($\varepsilon_r = 2.2$, tan δ = 0.0009 at 10 GHz) with a thickness of 1.57 mm. The patch and ground plane of the array consists of copper with 35μm thickness.

The reflection and radiation characteristics of the planar and conformal arrays are measured by using Anritsu MS4644A two-port vector network analyser. The measurement of the patterns is performed in the horizontal plane within $-90° \leq \theta \leq 90°$ angular range. The measured reflection coefficient of the arrays is given in Figure 14 within the frequency range of 8-12 GHz. The S_{11} variation of the planar and conformal array designed to radiate towards θ = -20° has lower than -10 dB approximately above 9 GHz, whereas the operating bandwidth is narrower for the other cases. The lower operating frequency planar and conformal is 10 GHz for the arrays designed to radiate $\theta = 15°$. The arrays that radiate boresight have narrower bandwidth of 650 MHZ between 10.5 GHz and 11.15 GHz.

Measured copolarized patterns of arrays are given for the planar and conformal arrays in Figure 15a and b, respectively. The blue solid line demonstrates the normalized pattern of the array that is designed to radiate boresight, whereas red dash-dotted and black dashed lines represent the patterns of the arrays designed to radiate towards



(a) (b)

Figure 12. Performance of the planar and conformal 1x4 phased arrays designed to radiate towards θ = -20° (a) reflection coefficient; (b) normalized gain patterns.

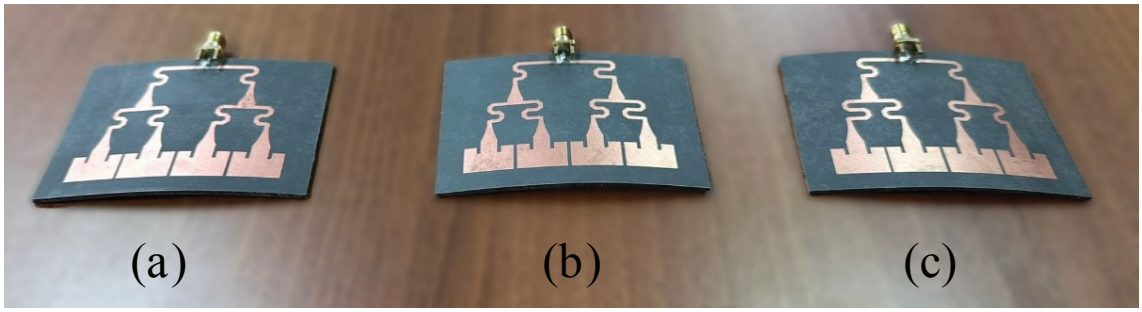


Figure 13. Prototype of the fabricated conformal arrays designed to radiate towards (a) θ = 15°; (b) θ = -20°; and (c) θ = 0°.

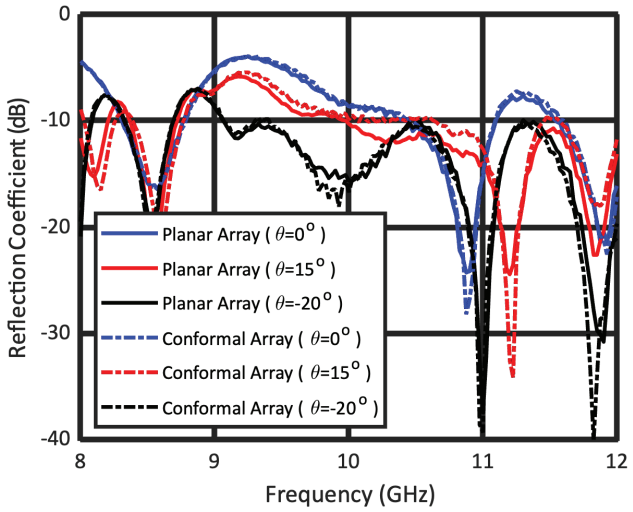
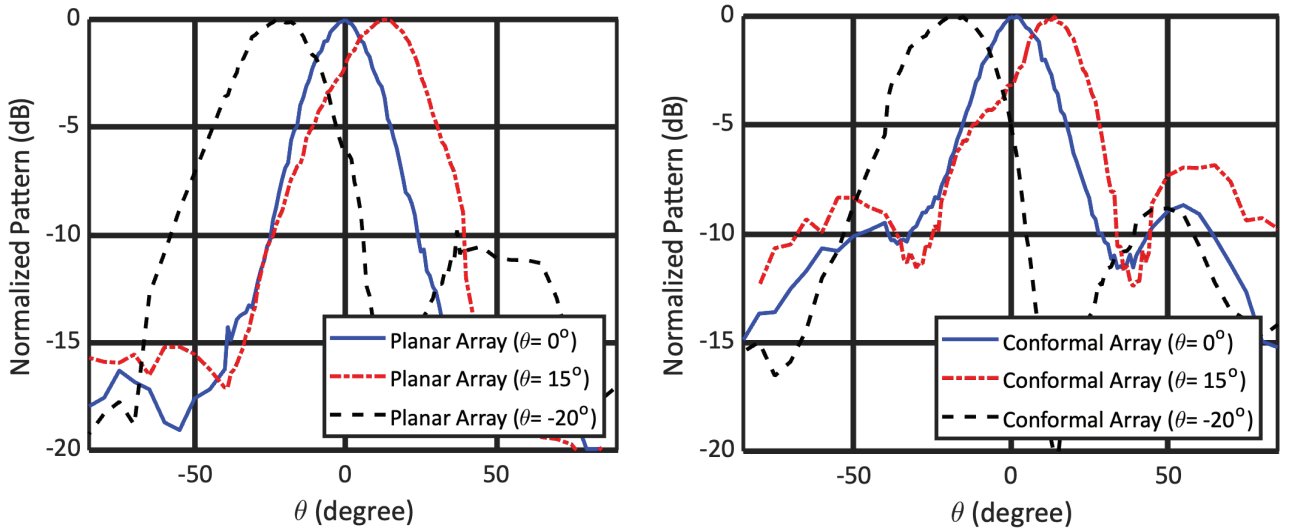


Figure 14. Measured reflection coefficient of the arrays.

θ = 0°, 15° and -20°, respectively. The main lobe directions of the patterns clearly show the beam steering performance of the 1 x 4 microstrip array for both planar and conformal arrays. Although the sidelobe level of the planar array that radiates to θ = -20° is close to 10 dB, the level is much higher for the other planar arrays. However, this is not the case for the conformal array. Bending the arrays results in higher side lobes, which reach 7.5 dB for the θ = 15° radiating conformal array. The gain of the planar arrays at 10 GHz are calculated as 11dBi, 10 dBi and 9 dBi for the θ = 0°, 15° and -20° radiation, respectively. Slight increase is observed at tha gain values for the conformal arrays. 12dBi, 10.1 dBi and 9.2 dBi are measured with the θ = 0°, 15° and -20° radiating conformal arrays, respectively. The increase of gain is attributed to the bending, which helps to enhance forward radiation and resuls in higher front to back ratios.



(a) (b)

Figure 15. Measured radiation patterns of the arrays (a) planar array; (b) conformal array.

CONCLUSION

This study presents the design, optimization, and experimental validation of a 1x4 PAA for UAV applications operating in the X-band. The antenna features beam steering capabilities, achieved through a T-junction power divider network and innovative S-shaped structures that enable continuous adjustment of the radiation direction. The performance of the PAA is characterized by a low reflection coefficient of -30.91 dB at 10.3 GHz, a bandwidth of approximately 250 MHz, and a peak gain of 10.28 dBi. Additionally, the array demonstrated reliable beam steering capabilities, maintaining high gain levels and good radiation patterns over a wide range of steering angles, with minor gain reductions (1.3 dBi for planar and 2 dBi for conformal arrays) when steered to off-boresight angles. The experimental results further validated the antenna's performance, showing consistent gain patterns and low sidelobe levels, with a gain enhancement in the conformal array due to its bent configuration, which improves forward radiation and front-to-back ratios. The proposed conformal phased array antenna design exhibits promising performance for UAV applications in the X-band, offering high directional gain, low sidelobes, and efficient beam steering capabilities. The proposed conformal phased array antenna has the capability to steer the beam dynamically. For altering the direction of the main beam smoothly, a phase shifter should be utilized in the application. Future work can explore the scalability of this design to larger arrays and its integration with advanced UAV platforms for enhanced operational capabilities. The proposed conformal antenna design is compact and lightweight, making it well-suited for integration into UAV systems with limited space and weight constraints.

AUTHORSHIP CONTRIBUTIONS

Authors equally contributed to this work.

DATA AVAILABILITY STATEMENT

The authors confirm that the data that supports the findings of this study are available within the article. Raw data that support the finding of this study are available from the corresponding author, upon reasonable request.

CONFLICT OF INTEREST

The authors declared no potential conflicts of interest with respect to the research, authorship, and/or publication of this article.

ETHICS

There are no ethical issues with the publication of this manuscript.

STATEMENT ON THE USE OF ARTIFICIAL INTELLIGENCE

Artificial intelligence was not used in the preparation of the article.

REFERENCES

[1] US Army Unmanned Aircraft Systems Center of Excellence. U.S. Army unmanned aircraft systems roadmap 2010-2035. United States: Department of the Army; 2010 Jan 1. Available at: https://rosap.ntl.bts.gov/view/dot/18249. Accessed November 4, 2026.

[2] Pakrooh R, Bohlooli A. Survey on unmanned aerial vehicles assisted Internet of Things: a service-oriented classification. Wirel Pers Commun 2021;119:1541–1575. [CrossRef]
[3] Unpaprom Y, Dussadeeb N, Ramaraj R. Modern agriculture drones: the development of smart farmers. Maejo University; 2018. p. 13–19.
[4] Ahirwar S, Swarnkar R, Bhukya S, Namwade G. Application of drone in agriculture. Int J Curr Microbiol Appl Sci 2019;8:2500–2505. [CrossRef]
[5] Hassija V, Chamola V, Gupta V, Jain S, Guizani N. A survey on supply chain security: application areas, security threats, and solution architectures. IEEE Internet Things J 2021;8:6222–6246. [CrossRef]
[6] Yi J, Zhang H, Li S, Feng O, Zhong G, Liu H. Logistics UAV air route network capacity evaluation method based on traffic flow allocation. IEEE Access 2023;11:63701–63713. [CrossRef]
[7] Du P, Shi Y, Cao H, Garg S, Alrashoud M, Shukla PK. AI-enabled trajectory optimization of logistics UAVs with wind impacts in smart cities. IEEE Trans Consum Electron 2024;70:3885–3897. [CrossRef]
[8] Hoseini SA, Hassan J, Bokani A, Kanhere SS. Trajectory optimization of flying energy sources using Q-learning to recharge hotspot UAVs. arXiv [Preprint] 2020;2003:12258. [CrossRef]
[9] Mohsan SAH, Khan MA, Noor F, Ullah I, Alsharif MH. Towards the unmanned aerial vehicles (UAVs): a comprehensive review. Drones 2022;6:147. [CrossRef]
[10] Restas A. Drone applications for supporting disaster management. World J Eng Technol 2015;3:316–321. [CrossRef]
[11] Gülüm Taş P, Taşkın A. Clustering approach with self-organizing maps for unmanned aerial vehicle response to post-earthquake fires: an application for Istanbul. Sigma J Eng Nat Sci 2024;42:692–700. [CrossRef]
[12] Ahmed F, Mohanta JC. Inspection of power transmission line insulators with autonomous quadcopter and SSD network. Sigma J Eng Nat Sci 2024;42:621–632. [CrossRef]
[13] Chamola V, Kotesh P, Naren AA, Gupta N, Guizani M. A comprehensive review of unmanned aerial vehicle attacks and neutralization techniques. Ad Hoc Netw 2021;111:102324. [CrossRef]
[14] Gupta L, Jain R, Vaszkun G. Survey of important issues in UAV communication networks. IEEE Commun Surv Tutor 2016;18:1123–1152. [CrossRef]
[15] Kim S, Cho H, Jung D. Circular formation guidance of fixed-wing UAVs using mesh network. IEEE Access 2022;10:115295–115306. [CrossRef]
[16] Eltayeb A, Rahmat MF, Basri MAM, Eltoum MAM, Mahmoud MS. Integral adaptive sliding mode control for quadcopter UAV under variable payload and disturbance. IEEE Access 2022;10:94754–94764. [CrossRef]
[17] Khawaja W, Guvenc I, Matolak DW, Fiebig UC, Schneckenburger N. A survey of air-to-ground propagation channel modeling for unmanned aerial vehicles. IEEE Commun Surv Tutor 2019;21:2361–2391. [CrossRef]
[18] Koru AT, Chang J, Wan Y. RSSI-based distributed control to align directional antenna pairs for UAV communication. IEEE ASME Trans Mechatron 2024;29:2877–2885. [CrossRef]
[19] Zhou S, Yang L, Zhao L, Bi G. Forward velocity extraction from UAV raw SAR data based on adaptive notch filtering. IEEE Geosci Remote Sens Lett 2016;13:1211–1215. [CrossRef]
[20] Montazeri S, González FR, Zhu X. Geocoding error correction for InSAR point clouds. Remote Sens 2018;10:1523. [CrossRef]
[21] Sun Z, Wu J, Yang J, Huang Y, Li C, Li D. Path planning for GEO-UAV bistatic SAR using constrained adaptive multiobjective differential evolution. IEEE Trans Geosci Remote Sens 2016;54:6444–6457. [CrossRef]
[22] Anterrieu E, Khazaal A. Brightness temperature map reconstruction from dual-polarimetric visibilities in synthetic aperture imaging radiometry. IEEE Trans Geosci Remote Sens 2008;46:606–612. [CrossRef]
[23] Niaz MW, Bhatti RA. High-isolation antenna system for X-band synthetic aperture radar. Wirel Pers Commun 2017;97:2741–2750. [CrossRef]
[24] Wang X, Wang Z, Pang C, Li Y. Review on polarimetric phased array radar technologies. Radar Sci Technol 2021;19:349–370.
[25] Bolam RC, Roque JPC, Vagapov Y, Day RJ, Slepchenkov M. A power budget analysis of an electrical uncrewed air vehicle (UAV) flying a basic mission profile. In: 2023 58th International Universities Power Engineering Conference (UPEC); Dublin, Ireland. IEEE; 2023. p. 1–5. [CrossRef]
[26] Deng Z, Wu F, Xu Y, Yang D, Xiao L. Energy minimization for radio map-based UAV pickup and delivery logistics system. IEEE Trans Veh Technol 2024;73:17893–17898. [CrossRef]
[27] Tutuncu B, Torpi H, Imeci ST. Directivity improvement of microstrip antenna by inverse refraction metamaterial. J Eng Res 2019;7:151–164. [CrossRef]
[28] Demircioglu E, Sazlı MH, İmeci ST, Sengul O. Soft computing techniques on multi-resonant antenna synthesis and analysis. Microw Opt Technol Lett 2013;55:2643–2648. [CrossRef]
[29] Imeci MY, Tütüncü B, Imeci ST. A 3-dB 90 degrees microstrip hybrid directional coupler at 2.27 GHz. AEU Int J Electron Commun 2023;163:154606. [CrossRef]
[30] Pandey GP, Kanaujia BK, Gautam AK, Gupta SK. Ultra-wideband L-strip proximity coupled slot loaded circular microstrip antenna for modern communication systems. Wirel Pers Commun 2013;70:139–151. [CrossRef]

[31] Reese MS, Balanis CA, Blncher CR, Barber GC. Modeling and simulation of a helicopter-mounted SATCOM antenna array. IEEE Antennas Propag Mag 2011;53:51–60. [CrossRef]

[32] Chen X, Yang L, Zhao J, Fu G. High-efficiency compact circularly polarized microstrip antenna with wide beamwidth for airborne communication. IEEE Antennas Wirel Propag Lett 2016;15:1518–1521. [CrossRef]

[33] Vazquez-Roy JL, Krozer V, Dall J. Wideband dual-polarization microstrip patch antenna array for airborne ice sounder. IEEE Antennas Propag Mag 2012;54:98–107. [CrossRef]

[34] Yang X, Liu X. Design of a wide-beam microstrip array antenna for automotive radar application. IEEE Access 2021;9:142340–142347. [CrossRef]

[35] Yi H, Wang Z, Xia D, Liu H, Li L. Periodic asymmetric trapezoidal perturbation microstrip antenna for millimeter-wave automotive radar sensors. IEEE Trans Antennas Propag 2023;71:1369–1377. [CrossRef]

[36] Qian J, Zhu H, Tang M, Mao J. A 24 GHz microstrip comb array antenna with high sidelobe suppression for radar sensor. IEEE Antennas Wirel Propag Lett 2021;20:1220–1224. [CrossRef]

[37] Dey S, Satheesh P, Keerthi MS, Kunju N, Dey S. Novel dual band high gain antenna array using aperture coupled feeding for X-band radar. In: First International Conference on Microwave, Antenna and Communication (MAC); Prayagraj, India; 2023. p. 1–5. [CrossRef]

[38] Koziel S, Ogurtsov S. Simulation-based design of microstrip linear antenna arrays using fast radiation response surrogates. IEEE Antennas Wirel Propag Lett 2015;14:759–762. [CrossRef]

[39] Liu Y, Wang H, Li K, Gong S. RCS reduction of a patch array antenna based on microstrip resonators. IEEE Antennas Wirel Propag Lett 2015;14:4–7. [CrossRef]

[40] Balanis CA. Antenna theory: analysis and design. 2nd ed. New York: John Wiley & Sons; 1996.

[41] Parker D, Zimmermann DC. Phased arrays - part 1: theory and architectures. IEEE Trans Microw Theory Tech 2002;50:678–687. [CrossRef]

[42] Banerjee D, Hashmi M, Ghannouchi F. Flexible ultra-high transformation ratio-based dual-band impedance transformer and its applications in a T-junction power divider. IET Microw Antennas Propag 2021;15:1553–1563. [CrossRef]

[43] Yang Y, Hu N, Xie W, Wang W, Wu Y. A compact triband impedance-transforming power divider with independent controllable power division ratios and enhanced bandwidths. IEEE Access 2019;7:25185–25194. [CrossRef]

[44] Sagar PP, Rajesh V, Altahan BR, Venkateswararao M, Ahammad SH, Smirani LK, et al. Design and analysis of rectangular circularly polarized array antenna for flexible IoT applications. Wirel Pers Commun 2023;130:1257–1275. [CrossRef]

[45] Liu WS. Miniaturized single-ended-to-balanced filtering power divider with high selectivity based on tri-mode resonator. IEEE Trans Circuits Syst II Express Briefs 2023;70:4048–4052. [CrossRef]

[46] Abbas S, Maqsood M, Shoaib N, Mehmood MQ, Zubair M, Massoud Y. A wideband RF power divider with ultra-wide harmonics suppression. IEEE J Microw 2023;3:1248–1257. [CrossRef]

[47] Barbadekar AB, Patil PM. Reconfigurable 1:4 Wilkinson power divider used in ISM band applications. In: Karrupusamy P, Balas VE, Shi Y, editors. Sustainable communication networks and application. Lecture Notes on Data Engineering and Communications Technologies. Vol. 93. Cham: Springer; 2022. [CrossRef]

[48] Dökmetaş B. S-Bant microstrip Wilkinson power divider design. [Article in Turkish]. J Sci Rep B 2021;4:8–18. [CrossRef]

[49] Zulkifli FY, Hidayat T, Basari, Rahardjo ET. Sidelobe level suppression using unequal four-way power divider for proximity coupled microstrip antenna. In: Asia-Pacific Microwave Conference Proceedings (APMC); 2013. p. 1166–1168. [CrossRef]